XXV. COMMUNICATIONS BIOPHYSICS*

Academic and Research Staff

Prof. P. R. Gray†
Prof. P. G. Katona
Prof. W. T. Peake‡
Prof. W. A. Rosenblith
Prof. W. M. Siebert
Prof. T. F. Weiss‡
Dr. J. S. Barlow**
Dr. G. O. Barnett¶
Dr. A. Borbely††
Dr. A. W. B. Cunningham‡‡
N. I. Durlach
Dr. O. Franzen***
Dr. R. D. Hall
Dr. G. Hellekant†††
Dr. N. Y. S. Kiang‡
Dr. R. G. Mark‡‡‡
Dr. M. Nomoto****
Dr. K. Offenloch††††
Dr. R. Rojas-Corona
Dr. G. F. Songster
R. M. Brown‡
A. H. Crist‡
W. F. Kelley
D. P. Langbein‡

Graduate Students

J. E. Berliner
G. von Bismarck
L. D. Braida
S. K. Burns
A. N. Chandra
H. S. Colburn
P. Demko
J. E. Evans
J. A. Freeman
J. J. Guinan, Jr.
R. M. Hershkowitz
H. S. Hsiao
E. G. Merrill
E. C. Moxon
M. J. Nahvi
R. E. Olsen
S. E. Portny
D. J-M. Poussart
I. H. Thomae
M. L. Wiederhold

Undergraduate Students

S. J. Bayer
J. F. Fairbanks
R. M. Farrell
S. Malgari
K. J. Sullivan

---

*This work was supported principally by the National Institutes of Health (Grant 2 PO1 GM-14940-01), and in part by the Joint Services Electronics Programs (U. S. Army, U. S. Navy, and U. S. Air Force) under Contract DA 28-043-AMC-02536(E), the National Aeronautics and Space Administration (Grant NsG-496), and the National Institutes of Health (Grant 2 RO1 NB-05462-03).

†Leave of absence, at General Atronics Corporation, Philadelphia, Pennsylvania.

‡Also at Eaton-Peabody Laboratory, Massachusetts Eye and Ear Infirmary, Boston, Mass.

**Research Affiliate in Communication Sciences from the Neurophysiological Laboratory of the Neurology Service of the Massachusetts General Hospital, Boston, Mass.

††Postdoctoral Fellow from the Brain Research Institute, University of Zurich, Zurich, Switzerland.

‡‡Associate in Pathology, Peter Bent Brigham Hospital.

***Postdoctoral Fellow from the Speech Transmission Laboratory, The Royal Institute of Technology, Stockholm, Sweden.

†††Postdoctoral Fellow from the Department of Physiology, Kungl. Veterinarskolan, Stockholm, Sweden.

‡‡‡Assistant Resident, Harvard Medical Service, Boston City Hospital, Boston, Mass.

****Public Health Service International Postdoctoral Research Fellow, from the Department of Physiology, Tokyo Medical and Dental University, Tokyo, Japan.

¶Associate in Medicine, Department of Medicine, Harvard Medical School, and Director, Laboratory of Computer Science, Massachusetts General Hospital.

††††Public Health Service International Postdoctoral Fellow from the Max Planck Institut for Brain Research, Frankfurt, Germany.

A. ON EXTRACELLULAR POTENTIALS IN A VOLUME CONDUCTOR

This report is concerned with the extracellular potential generated by a cell situated in a volume conductor. A derivation of the results will be followed by (i) a brief discussion of the results obtained by others, and (ii) a discussion of related problems concerned with cellular potentials.

Consider a cell whose membrane separates two ionic solutions: the inner solution defines a volume, τ_i, that is bounded by the inner surface of the membrane, S_{m_i}, and the outer solution defines a volume, τ_o, that is bounded by the outer surface of the membrane, S_{m_o}, and by an insulating boundary, S_o. The inner and outer ionic solutions are assumed to be characterized by their conductivities, σ_i and σ_o, respectively. Furthermore, we assume that quasi-statics applies and, therefore, that the electric field may be derived from the gradient of the electric potential.

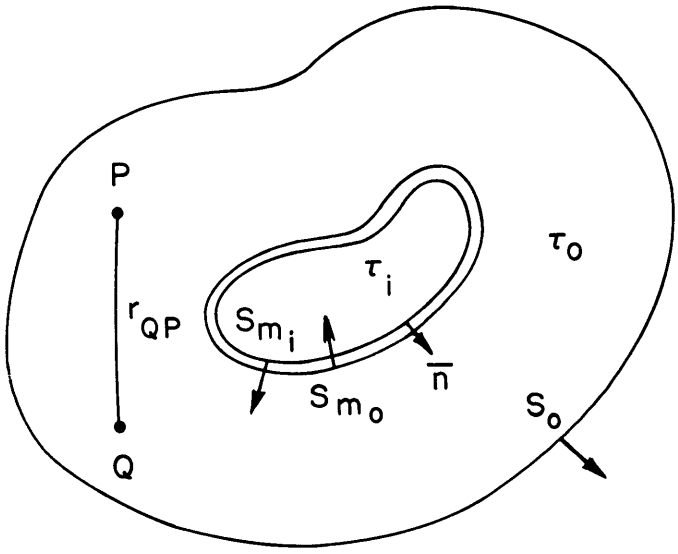

Fig. XXV-1. Arrows indicate the directions of the outward normal vectors to the surfaces S_{m_i}, S_{m_o}, S_o and the unit vector $\bar{n}$.

Suppose that two potential functions ϕ and ψ are defined on τ_i and τ_o, where ϕ satisfies Laplace's equation on τ_i and τ_o,

$$\nabla^2\phi = 0 \qquad \text{on } \tau_i, \tau_o.$$

Now consider the volume integral on the function $\nabla \cdot (\psi\nabla\phi)$. By Gauss' Theorem

$$\int_{\tau_i} \nabla \cdot (\psi \nabla \phi)\, d\tau = \int_{S_{m_i}} \psi \nabla \phi \cdot \overline{dS}, \tag{1}$$

where the volume integral on the left is taken over the volume τ_i, and the surface integral on the right is taken over the surface S_{m_i} which bounds τ_i. The positive direction of a differential element of surface area on S_{m_i} is taken as the outward normal to the surface, as shown in Fig. XXV-1.

But

$$\nabla \cdot (\psi \nabla \phi) = \nabla \psi \cdot \nabla \phi + \psi \nabla^2 \phi. \tag{2}$$

Therefore

$$\int_{\tau_i} (\nabla \psi \cdot \nabla \phi + \psi \nabla^2 \phi)\, d\tau = \int_{S_{m_i}} \psi \nabla \phi \cdot \overline{dS}. \tag{3}$$

Now consider the volume integral on the function $\nabla \cdot (\phi \nabla \psi)$. By an identical argument, this yields

$$\int_{\tau_i} (\nabla \phi \cdot \nabla \psi + \phi \nabla^2 \psi)\, d\tau = \int_{S_{m_i}} \phi \nabla \psi \cdot \overline{dS}. \tag{4}$$

Now subtracting Eq. 4 from Eq. 3 yields

$$\int_{\tau_i} (\psi \nabla^2 \phi - \phi \nabla^2 \psi)\, d\tau = \int_{S_{m_i}} (\psi \nabla \phi - \phi \nabla \psi) \cdot \overline{dS}. \tag{5}$$

Equation 5 is known as Green's theorem (see for instance, Stratton[1]), and for $\nabla^2 \phi = 0$ it yields

$$-\int_{\tau_i} \phi \nabla^2 \psi\, d\tau = \int_{S_{m_i}} (\psi \nabla \phi - \phi \nabla \psi) \cdot \overline{dS}. \tag{6}$$

By an analogous argument, the volume integral on τ_o is related to the surface integral bounding the volume

$$-\int_{\tau_o} \phi \nabla^2 \psi\, d\tau = \int_{S_{m_o}, S_o} (\psi \nabla \phi - \phi \nabla \psi) \cdot \overline{dS}. \tag{7}$$

Let $\psi = \frac{1}{r_{QP}}$, where r_{QP} is the distance from a source point, Q, located at $\overline{r}_Q$ to a point of observation, P, located at $\overline{r}_P$. Now it can be shown (See Panofsky and Phillips[2]) that

$$\nabla^2 \frac{1}{r_{QP}} = -4\pi u_o(r_{QP}),$$

where the Laplacian operator is evaluated at the field point, P, and $u_o(r_{QP})$ is the unit impulse having the property

$$\int_\tau f(\overline{r}_Q)\, u_o(r_{QP})\, d\tau = f(\overline{r}_P) \qquad \text{if } \tau \text{ included the point for which } r_{QP} = 0.$$

Substitution for ψ in Eqs. 6 and 7 yields

$$4\pi\phi(\overline{r}_P) = \int_{S_{m_i}} \left(\frac{1}{r_{QP}} \nabla\phi - \phi\nabla \frac{1}{r_{QP}}\right) \cdot \overline{dS} \quad \text{for P in } \tau_i \tag{8}$$

$$0 = \int_{S_{m_i}} \left(\frac{1}{r_{QP}} \nabla\phi - \phi\nabla \frac{1}{r_{QP}}\right) \cdot \overline{dS} \quad \text{for P not in } \tau_i \tag{9}$$

and

$$4\pi\phi(\overline{r}_P) = \int_{S_{m_o}, S_o} \left(\frac{1}{r_{QP}} \nabla\phi - \phi\nabla \frac{1}{r_{QP}}\right) \cdot \overline{dS} \quad \text{for P in } \tau_o \tag{10}$$

$$0 = \int_{S_{m_o}, S_o} \left(\frac{1}{r_{QP}} \nabla\phi - \phi\nabla \frac{1}{r_{QP}}\right) \cdot \overline{dS} \quad \text{for P not in } \tau_o. \tag{11}$$

Consider an observation point in τ_o, then add Eq. 10 to Eq. 9 multiplied by an arbitrary constant, a, to obtain

$$4\pi\phi(r_P) = \int_{S_{m_o}, S_o} \left(\frac{1}{r_{QP}} \nabla\phi - \phi\nabla \frac{1}{r_{QP}}\right) \cdot \overline{dS}$$

$$+ a \int_{S_{m_i}} \left(\frac{1}{r_{QP}} \nabla\phi - \phi\nabla \frac{1}{r_{QP}}\right) \cdot \overline{dS} \tag{12}$$

for any point in τ_o. Integrals to be evaluated on the inner and outer surfaces of the membrane can be expressed in terms of the potential on the inner surface of the membrane, V_i, the potential on the outer surface of the membrane, V_o, and the membrane current density, J_m. Assuming that the normal component of current is continuous through the membrane, and assuming the convention that the current density is positive when it flows from the inside to the outside of the membrane, one obtains

$$4\pi\phi(\bar{r}_P) = \int_{S_{m_o}} \left(-\frac{1}{r_{QP}} \frac{\bar{J}}{\sigma_o} - V_o \nabla \frac{1}{r_{QP}} \right) \cdot \overline{dS}$$

$$+ \alpha \int_{S_{m_i}} \left(-\frac{1}{r_{QP}} \frac{\bar{J}}{\sigma_i} - V_i \nabla \frac{1}{r_{QP}} \right) \cdot \overline{dS}$$

$$+ \int_{S_o} \left(\frac{1}{r_{QP}} \nabla\phi - \phi \nabla \frac{1}{r_{QP}} \right) \cdot \overline{dS}, \qquad (13)$$

where $\nabla\phi = -\frac{\bar{J}}{\sigma}$ in the volume conductors, $\bar{J}$ is the current density, and σ is the conductivity (σ_i in τ_i and σ_o in τ_o).

It is useful to combine the two terms that correspond to integrals over the two surfaces of the membrane. Since cellular membranes are very thin (thicknesses of the order of 100 Å) as compared with both the radius of curvature of the membrane and the observation distance, it seems reasonable to assume[3,4] that distances from the inner and outer surfaces of the membrane to any observation point are approximately equal and that the surface elements, $\overline{dS}$, over the inner and outer surfaces differ only in the directions of the outward normals. The differential elements of surface area on S_{m_i} and S_{m_o} can be expressed in terms of the vector $\bar{n}$ da, where $\bar{n}$ is a unit vector normal to the membrane and pointing from inside to outside, and da is a scalar, differential element of area.

Also, $\bar{J} \cdot \bar{n} = J_m$ and $\left(\nabla \frac{1}{r_{QP}} \right) \cdot \bar{n}$ is written as $\nabla_n \frac{1}{r_{QP}}$ to yield

$$4\pi\phi(\bar{r}_P) = \int_{S_m} \left(\frac{1}{r_{QP}} J_m \left(\frac{1}{\sigma_o} - \frac{\alpha}{\sigma_i} \right) + \left(V_o - \alpha V_i \right) \nabla_n \frac{1}{r_{QP}} \right) da$$

$$+ \int_{S_o} \left(\frac{1}{r_{QP}} \nabla\phi - \phi \nabla \frac{1}{r_{QP}} \right) \cdot \overline{dS}. \qquad (14)$$

Since α is an arbitrary constant, a variety of expressions can be obtained from Eq. 14, depending upon the choice of α. If α is chosen to equal $\frac{\sigma_i}{\sigma_o}$, then Eq. 14 becomes

$$4\pi\phi(\bar{r}_P) = \int_{S_m}\left(\left(V_o - \frac{\sigma_i}{\sigma_o} V_i\right) \nabla_n \frac{1}{r_{QP}}\right) da$$

$$+ \int_{S_o}\left(\frac{1}{r_{QP}} \nabla\phi - \phi\nabla \frac{1}{r_{QP}}\right) \cdot \overline{dS}. \qquad (15)$$

From Eq. 15 the extracellular potential can be calculated from the distribution of the inner and outer surface potentials on the membrane. Equation 15 has previously been derived by Geselowitz,[3] Plonsey,[4, 5] and Stevens.[6]

For $\alpha = 1$, define $V_m = V_i - V_o$ and one can obtain an expression for the extracellular potential in terms of the membrane current, J_m, and the membrane voltage, V_m:

$$4\pi\phi(\bar{r}_P) = \int_{S_m}\left(\frac{1}{r_{QP}} J_m\left(\frac{1}{\sigma_o} - \frac{1}{\sigma_i}\right) - V_m \nabla_n \frac{1}{r_{QP}}\right) da$$

$$+ \int_{S_o}\left(\frac{1}{r_{QP}} \nabla\phi - \phi\nabla \frac{1}{r_{QP}}\right) \cdot \overline{dS}. \qquad (16)$$

Equation 16 was obtained by Geselowitz.[3]

Other interesting expressions can be derived from Eq. 14, and by making suitable approximations (for instance, by assuming $V_o \ll V_i$), other useful expressions can be obtained. The papers of Geselowitz,[3] Plonsey,[4, 5] and Stevens[6] should be consulted for discussions of those expressions. Geselowitz[3] has also considered the case of an inhomogeneous volume conductor surrounding a cell. The inhomogeneity is represented by allowing for the presence of volumes of conductivity other than σ_o in τ_o. Equation 14 can be generalized to include this kind of inhomogeneity in the volume conductor by addition to Eq. 14 of terms of the form

$$\int_{S_k}\left(\frac{1}{r_{QP}} \nabla\phi - \phi\nabla \frac{1}{r_{QP}}\right) \cdot \overline{dS},$$

where the integral is evaluated on the surface, S_k, of the k^{th} body, τ_k.

The field-theoretic approach to the representation of bioelectric potentials has made some contact with problems in electrophysiology. For tutorial purposes, we would like to review briefly and comment upon these problems.

Although we have made no thorough literature search to support this statement,

Craib[7] may have been the first investigator to report on the differences in the wave shape of extracellular potentials recorded from a strip of muscle placed in a limited and in an extended volume conductor. Craib[7] noted that with monopolar recording, the extracellular compound action potential recorded from a muscle in a limited volume conductor in response to a brief electric stimulus was monophasic. The response of the same muscle immersed in an extensive volume conductor was triphasic. A comprehensive treatment of the theoretical problem was given by Lorente de Nó,[8] based upon a paper by Helmholtz[9] on potentials in a volume conductor (for a modern treatment of the more general problem of potentials in a volume conductor see Stratton[1]). Lorente de Nó[8] also performed experiments on frog sciatic nerves and was able to account for the extracellular potentials recorded in a large volume of saline solution on the basis of the theory and recordings made with the nerve in a limited volume conductor. Håkansson[10] has reported on a similar experiment performed on single muscle fibers. In this case, intracellular and extracellular potentials were recorded simultaneously. The results of all of these investigations indicates that one can account in at least a qualitative manner for the triphasic potential recorded from nerve and muscle bundles and fibers in extended volume conductors. Qualitative theoretical arguments (in addition to the formal treatments cited previously) to account for this observation have been given by Mauro,[11] Offner,[12] and Woodbury.[13]

A field-theoretic approach might conceivably also have relevance for the justification of the distributed electric circuit representation of axons and muscle fibers (often referred to as the core conductor model). A start in this direction has been made by Clark and Plonsey.[14] For instance, the circuit-theoretic approach leads to the result that the extracellular potential is proportional to the membrane potential in the extrapolar region.[15] This result appears to be in substantial agreement with experimental data obtained with the fiber immersed in a limited volume conductor (a condition that is realized experimentally by placing the fiber in air, oil or a de-ionized sucrose solution, and recording from the surface of the fiber to which a thin film of ionic solution presumably still adheres). Such a result should, in principle, be derivable directly from the field-theoretic approach.

T. F. Weiss

References

1. J. A. Stratton, Electromagnetic Theory (McGraw-Hill Book Company, New York, 1941).

2. W. K. H. Panofsky and M. Phillips, Classical Electricity and Magnetism (Addison-Wesley Publishing Company, Reading, Mass., 1955).

3. D. B. Geselowitz, "On Bioelectric Potentials in an Inhomogeneous Volume Conductor," Biophys. J. 7, 1-11 (1967).

4. R. Plonsey, "An Extension of the Solid Angle Potential Formulation for an Active Cell," Biophys. J. 5, 663-667 (1965).

5. R. Plonsey, "Volume Conductor Fields of Action Currents," Biophys. J. 4, 317-328 (1964).

6. C. F. Stevens, Neurophysiology: A Primer (John Wiley and Sons, Inc., New York, 1966).

7. W. H. Craib, "A Study of the Electrical Field Surrounding Skeletal Muscle," J. Physiol. 66, 49-73 (1928).

8. R. Lorente de Nó, "Analysis of the Distribution of the Action Currents of Nerve in Volume Conductors," Studies Rockefeller Inst. Med. Res. 132, 384-477 (1947).

9. H. von Helmholtz, "Ueber einige Gesetze der Vertheilung elektrischer Ströme in körperlichen Leitern mit Anwendung auf die thierisch-elektrischen Versuche," Poggendorff's Ann. 89, 211-233; 353-377 (1853). Reprinted in H. Helmholtz Wiss. Abhandl. 1, 475-519 (1883) (Johann Ambrosius Barth, Leipzig).

10. C. H. Håkansson, "Action Potentials Recorded Intra- and Extra-cellularly from Isolated Frog Muscle Fibre in Ringer's Solution and in Air," Acta Phys. Scand. 39, 291-312 (1957).

11. A. Mauro, "Properties of Thin Generators Pertaining to Electrophysiological Potentials in Volume Conductors," J. Neurophysiol. 23, 132-143 (1960).

12. F. F. Offner, "The Tri-phasic Action Potentials," Electroenceph. Clin. Neurophysiol. 6, 507-508 (1954).

13. J. W. Woodbury, "Potentials in a Volume Conductor," pp. 85-91 in Physiology and Biophysics, T. C. Ruch and H. D. Patton (eds.) (W. B. Saunders Company, Philadelphia, 19th edition, 1965).

14. J. Clark and R. Plonsey, "A Mathematical Evaluation of the Core Conductor Model," Biophys. J. 6, 95-112 (1966).

15. A. L. Hodgkin and W. A. H. Rushton, "The Electrical Constants of a Crustacean Nerve Fibre," Proc. Roy. Soc. (London) B133, 444-479 (1946).

B. PULSE-DURATION MODULATOR

[This report summarizes an S. B. thesis submitted to the Department of Electrical Engineering, M. I. T., June 1967.]

A simple circuit has been developed for tape recording of bioelectric signals. It is a pulse-duration modulation system that multiplexes two inputs. The frequency range is from DC to 500 Hz. The basic operation of the system is illustrated in Fig. XXV-2. With a positive input on #1 and #2, C_1 charges at a uniform rate until its voltage is equal to input #2, at which point C_2 begins to charge, again at a uniform rate until its voltage reaches the level of input #1. Then the cycle repeats itself. Output is in the form of a pulse train, the "high" pulse length is proportional to input #2, the "low" pulse length is proportional to input #1.

Differential inputs have been added to permit bipolar inputs of ±1 volt, with output pulse lengths from 50 to 450 msec.

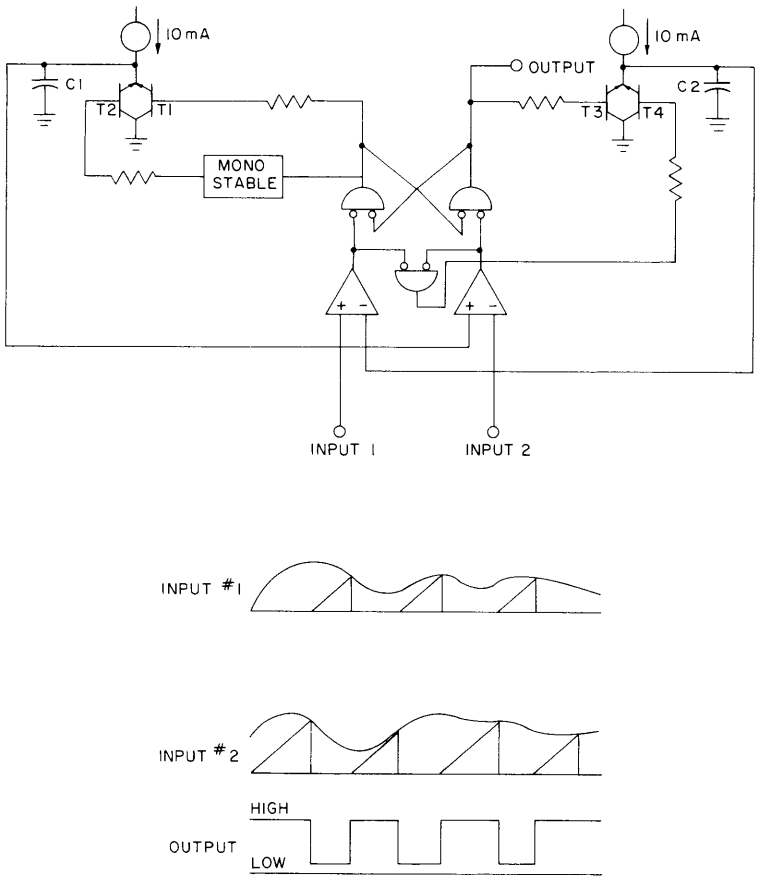

Fig. XXV-2. Illustrating system operation.

Tests have shown a linearity of better than 1 per cent and a less than 5 per cent change in output pulse length for temperature variations from -35°C to +90°C.

K. J. Sullivan

C. PSYCHOPHYSICS

Recent work in psychophysics has consisted in (a) performing further experiments on binaural signal detection, (b) initiating experiments on interaural just-noticeable differences and time-intensity trading, (c) examining the possibility of predicting interaural jnd's from auditory nerve data, (d) determining the effect of duration on the discrimination of periodicity pitch, (e) exploring the extent to which detection, discrimination, and absolute identification performance can be predicted from magnitude estimation data, (f) studying uncertainty estimates in absolute identification, (g) examining sequential dependence in auditory intensity discrimination, (h) gaining familiarization with problems in the study of short-term memory of sounds, (i) constructing a stimulus-timing device, (j) constructing a detection and triggering device for bat signals,

(k) writing programs on the PDP-4 computer for processing various types of psychophysical data, and (l) building interface equipment for the PDP-4 computer that will increase its useability for on-line experiments. A few of these items are discussed here. The rest will be discussed in future reports.

N. I. Durlach

1. BINAURAL SIGNAL DETECTION

Further experiments have been performed on the binaural unmasking of tones masked by random noise as a function of noise bandwidth and interaural phase. In all cases, the tone and noise were identical from ear to ear, except for phase. The results are reported in terms of binaural masking-level differences (BMLD's), where the homophasic configuration (tone and noise identical from ear to ear) is taken as the reference condition. The BMLD's are denoted $B(\phi_s|\phi_n)$, where ϕ_s is the interaural phase of the tone, and ϕ_n that of the noise. The symbols f_o, W, and P denote the frequency of the tone, and bandwidth of the noise, and the total power of the noise, respectively.

The motivation for performing these experiments was (i) to explore further the increase in BMLD's with a decrease in bandwidth previously reported at f_o = 500 Hz by Langford and Jeffress,[1] Bourbon and Jeffress,[2] and Riezenman[3]; (ii) to determine the way in which the "flattening" phenomenon that occurs in $B(0|\phi_n)$ for $f_o < 500$ Hz (discovered by Jeffress, Blodgett, and Deatherage,[4] and studied further by Durlach[5] and Rabiner, Laurence, and Durlach[6]) is influenced by choosing values of ϕ_s other than zero; (iii) to evaluate the prediction (implied by the "decorrelation-factor" hypothesis considered by Rabiner, Laurence, and Durlach[6]) that the flattening in $B(0|\phi_n)$ decreases as the bandwidth of the noise is decreased; and (iv) to evaluate the prediction by Green[7] concerning the bandwidth dependence of $B(180°|0)$ at the lower frequencies. Most of the measurements in the present set of experiments were made for frequencies, f_o, in the range $250 \leq f_o \leq 400$ Hz, power levels P in the range 85 dB $\leq$ P $\leq$ 90 dB SPL, and for bandwidths W of 4, 250, and 1000 Hz. A few measurements were also made for f_o covering the range $250 \leq f_o \leq 4000$ Hz and bandwidths, W, of 3 and 1000 Hz.

The results of these experiments show that the increase in BMLD's with a decrease in bandwidth occurs at all frequencies in the range $250 \leq f_o \leq 4000$ Hz, and that previous predictions for the bandwidth dependence are inadequate. Data from a single subject in the principal low-frequency experiment are shown by the points in Fig. XXV-3. The solid and dashed curves are based on the equalization and cancellation (EC) model.[5-10] The solid curves are derived from the preliminary version of the model and are computed from the formula

$$B(\phi_s|\phi_n) = \frac{k - \cos(\phi_s - \phi_n)}{k - 1}, \qquad (1)$$

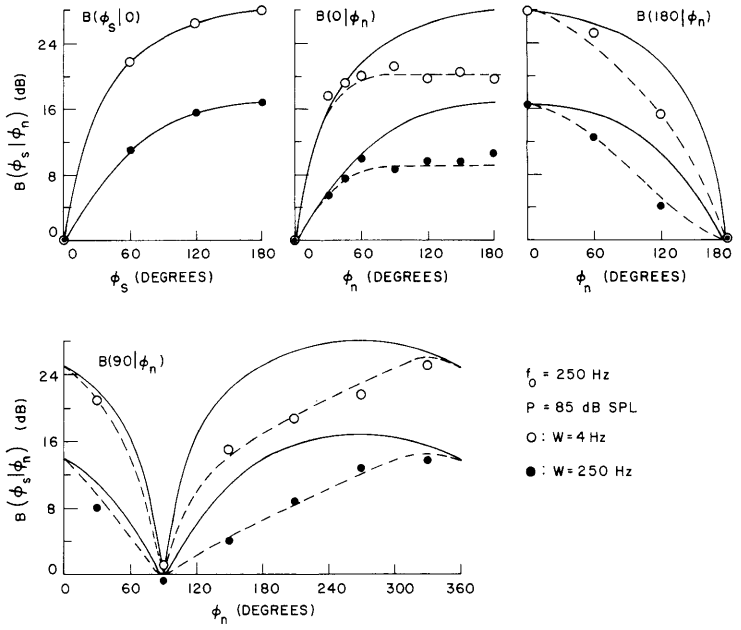

Fig. XXV-3. $B(\phi_s|\phi_n)(W)$ for a single subject at f_o = 250 Hz and P = 85 dB SPL. [The dashed and solid curves coincide for $B(\phi_s|0)(W)$.]

where k = 1.0450 for W = 250 Hz, and k = 1.0033 for W = 4 Hz. In previous work, it has been shown that Eq. 1 is capable of providing a precise description of $B(\phi_s|0)$, but that it is inadequate for describing $B(0|\phi_n)$ at frequencies $f_o < 500$ Hz and values of ϕ_n greater than $H/2\pi f_o$, where $H \approx 0.7$ msec. These results are again confirmed by the present experiments. The phenomena that are evident in Fig. XXV-3 and about which there are very little previous data are (i) the growth of BMLD's with a decrease in W; (ii) the manner in which the flattening in $B(0|\phi_n)$ is transformed when ϕ_s takes on values different from zero; and (iii) the way in which the deviations between the data and the preliminary model are related to noise bandwidth. Roughly speaking, the increase in the BMLD's at f_o = 250 Hz as W is decreased from 250 Hz to 4 Hz can be summarized by noting that $B(\phi_s|\phi_n)(W=4)/B(\phi_s|\phi_n)(W=250) \approx 10$ dB for all cases tested in which $\phi_s - \phi_n \neq 0$, and that $B(\phi_s|\phi_n) \approx 0$ dB when $\phi_s - \phi_n = 0$, independent of W. In considering these results, it should be recalled that BMLD's vary very slowly with power level, so that the increase in the power level at the output of the critical band produced by decreasing W from 250 Hz to 4 Hz (with P held constant) has a very small effect on the BMLD's, and the increase of the BMLD's can be ascribed almost entirely to the bandwidth effect itself.

According to the revision of the EC model proposed by Rabiner, Laurence, and Durlach,[6] the ratio $B(180°|0)/B(0|180°)$, or more generally, the difference between

the curves for $B(\phi_s | 0)$ and $B(0 | \phi_n)$, should decrease as W is decreased. This prediction is clearly contradicted by the data. Similarly, the prediction of Green[7] that $B(180° | 0)$ is proportional to $(3 + 2WT)^{-1/2}$, where W is measured at the output of the critical band, and T is the integration time of the system (or the signal duration if this duration is shorter than the integration time), has been found inadequate. Whereas the bandwidth effect has been found to be approximately 10 dB, Green's formula predicts an effect of less than 5 dB.

The dashed curves in Fig. XXV-3 have been derived by assuming that k is independent of ϕ_s and that it depends on ϕ_n and W in such a way that the deviation of k from unity (i.e., the difference between the "real" k and the k that would occur if the system performed perfectly) can be factored into a product of a bandwidth factor and a noise-phase factor. The formula derived from this assumption is identical to Eq. 1, except that k must be replaced by $k = 1 + K_1(W)\, K_2(\phi_n)$:

$$B(\phi_s | \phi_n)(W) = \frac{1 + K_1(W)\, K_2(\phi_n) - \cos(\phi_s - \phi_n)}{K_1(W)\, K_2(\phi_n)}. \tag{2}$$

The dashed curves are obtained by choosing the function $K_1(W)\, K_2(\phi_n)$ to fit the data in Fig. XXV-3, and the values of $K_1(W)\, K_2(\phi_n)$ corresponding to these curves are shown in Fig. XXV-4. On the whole, the assumption that k is of the form $k = 1 + K_1(W) K_2(\phi_n)$

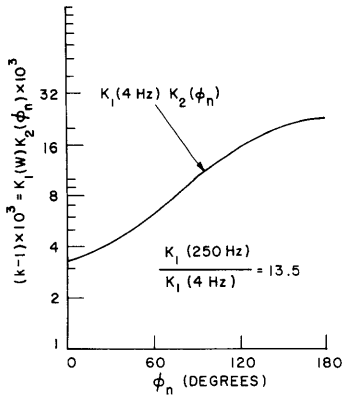

Fig. XXV-4. Values of $K_1(W)\, K_2(\phi_n)$ corresponding to the dashed curves in Fig. XXV-3.

has been found capable of providing an excellent representation of the data. Although the function $k = 1 + K_1(W)\, K_2(\phi_n)$ obviously permits considerable flexibility, it is much more restrictive than the function $k = k(W, \phi_n, \phi_s)$ that corresponds to a pure fitting procedure without any structural constraints. Furthermore, it is the author's conjecture that similarly good results would be obtained for configurations in which the interaural amplitude ratio a_s of the tone is varied. In other words, we believe that the success of the model for the case $B(a_s, \phi_s | 0)$ demonstrated by Colburn and Durlach[9] can be extended to the more general case $B(a_s, \phi_s | \phi_n)(W)$, provided k is allowed to vary with

W and ϕ_n, as in the present analysis. The prediction for this more general case is given by

$$B(a_s, \phi_s | \phi_n)(W) = \text{Maximum} \left\{ \frac{[1+K_1(W)\, K_2(\phi_n)]\left(1+a_s^{6-4j}\right) - 2a_s^{3-2j} \cos(\phi_s-\phi_n)}{2K_1(W)\, K_2(\phi_n)} \right\}, \quad (3)$$

where $j = 1$ when $a_s \leq 1$, and $j = 2$ when $a_s > 1$. In order to determine the accuracy of this generalization, and in order to determine whether or not the results on $K_1(W)\, K_2(\phi_n)$ can be given any meaning other than that associated with the fitting of the data on BMLD's, requires further work. A paper on the present results is being prepared for publication. Details on some of this work can be found in the author's S. M. thesis.

P. J. Metz

References

1. T. L. Langford and L. A. Jeffress, "Effect of Noise Crosscorrelation for a Narrow-band Masking Noise on the Detection of a Tonal Signal," J. Acoust. Soc. Am. 36, 1042(A) (1964).
2. W. T. Bourbon and L. A. Jeffress, "Effect of Bandwidth of Masking Noise on Detection of Homophasic and Antiphasic Tonal Signals," J. Acoust. Soc. Am. 37, 1180(A) (1965).
3. M. J. Riezenman, "Binaural Unmasking as a Function of the Bandwidth of the Masking Noise," S. B. Thesis, Department of Electrical Engineering, M.I.T., June 1965.
4. L. A. Jeffress, H. C. Blodgett, and B. H. Deatherage, "Masking and Interaural Phase. II. 167 cps," J. Acoust. Soc. Am. 34, 1124-1126 (1962).
5. N. I. Durlach, "Equalization and Cancellation Theory of Binaural Masking-Level Differences," J. Acoust. Soc. Am. 35, 1206-1218 (1963).
6. L. R. Rabiner, C. L. Laurence, and N. I. Durlach, "Further Results on Binaural Unmasking and the EC Model," J. Acoust. Soc. Am. 40, 62-70 (1966).
7. D. M. Green, "Signal-Detection Analysis of Equalization and Cancellation Model," J. Acoust. Soc. Am. 40, 833-838 (1966).
8. N. I. Durlach, "Note on Binaural Masking-Level Differences as a Function of the Interaural Correlation of the Masking Noise," J. Acoust. Soc. Am. 36, 1613-1617 (1964).
9. H. S. Colburn and N. I. Durlach, "Time-Intensity Relations in Binaural Unmasking," J. Acoust. Soc. Am. 38, 93-103 (1965).
10. N. I. Durlach, "On the Application of the EC Model to Interaural JND's," J. Acoust. Soc. Am. 40, 1392-1397 (1966).

2. DETECTION AND TRIGGERING DEVICE FOR RESEARCH ON BAT-ECHOLOCATION SYSTEMS

In the studies of bat sonar being carried out by F. A. Webster,[1] it is often necessary to turn on equipment (such as a camera or jammer) at a precise instant in time

determined by the activity of the bat. In most previous work, this instant has been determined by visual or acoustical observation of the bat by the experimenter, and the turning-on of the equipment has been accomplished manually by pressing a button. Inasmuch as many of the bat's operations are performed very quickly, this procedure has often proved inadequate.

In order to improve this situation, it was necessary to build a trigger that would fire the auxiliary equipment automatically when the bat's behavior reached some predetermined criterion. The behavioral parameter suggested by Webster as the most useful was the repetition frequency of the bat's emitted signal. Specifically, it was suggested that a device be built that would trigger the auxiliary equipment when the repetition rate exceeded a certain preset value.

Such a device has now been constructed and consists of an analog circuit for detecting bat pulses in the presence of noise and echoes, and a digital circuit for determining the pulse repetition frequency. We have attempted to eliminate echoes by providing an adjustable detection threshold and a "blanking gate" that gates off the received signal for a certain adjustable period (4-10 msec) after the threshold has been exceeded. The optimal settings of the threshold and the blanking gate depend on the strength of the bat signal and on the acoustical environment. The device is also adjustable with respect to both the repetition rate required to fire the trigger pulse (10 pulses/sec to 250 pulses/sec) and the number of consecutive pulses that must satisfy the repetition rate criterion (2-7). Once the trigger pulse has been fired, it must be reset manually by pressing a button before it will fire again.

Further details may be found in the author's S. B. thesis.

J. T. Fairbanks

References

1. See, for example, F. A. Webster and N. I. Durlach, "Echolocation Systems of the Bat; Progress Report on Experimental Studies Conducted at F. A. Webster's Laboratory (1 Nov. 1961 – 1 Sept. 1962)," Report 41G-3, Lincoln Laboratory, M. I. T., 1963; F. A. Webster, "Active Energy Radiating Systems: The Bat and Ultrasonic Principles II; Acoustical Control of Airborne Interceptions by Bats," Proc. Inter. Cong. on Tech. and Blindness, Vol. 1, 49-135; 1963; F. A. Webster, "Bat-Type Signals and Some Implications," Chapter 25 in Bennet, Degan, and Spiegal (eds.), Human Factors in Technology, McGraw-Hill, New York, 1963; F. A. Webster and O. G. Brazier, "Experimental Studies on Target Detection, Evaluation, and Interception by Echolocating Bats," AMRL-TR-65-172, Air Force Systems Command, Wright-Patterson Air Force Base, Ohio, 1965.

3. STIMULUS TIMER

A stimulus timer (CBL-45) has been constructed to provide timing pulses for a wide variety of psychoacoustic experiments. It has 9 dual independent pulse outputs for

stimulus control. One of the dual outputs is a positive 3-volt pulse with respect to ground at an impedance of 100 ohms, while the other output is a 60-volt negative pulse with respect to ground at an impedance of 1000 ohms. Each of 8 outputs can be varied in time, independently, with respect to the 9^{th} output by means of 4 decade switches. The repetition period can be varied from 1 msec to 1000 seconds. Each of the 8 outputs can be varied in time with respect to the 9^{th} output in 0.1-msec steps up to 1 sec, 1.0-msec steps up to 10 sec, 10-msec steps up to 100 sec, and 100-msec steps up to 1000 seconds. This unit will replace a substantial number of Tektronix units (161 and 162) now being used for stimulus timing. Its primary advantage over the Tektronix equipment is that it is easier to operate, and thus reduces experimental "set-up" time.

W. F. Kelley

D. CAPACITIVE-TRANSDUCER INSTRUMENT FOR MEASURING DISPLACEMENT OF THE MIDDLE EAR IN ANIMALS

Several capacitive transducer systems have been developed for measuring vibrations in the middle ear.[1-5] The measurement involves detection of the change in capacitance between the vibrating part and the probe of the instrument. In one approach,[3] the probe capacitance constitutes a series coupling impedance between a sinusoidal radiofrequency constant-voltage generator and the input of the measuring channel; the changing impedance causes amplitude modulation of the carrier signal. Other workers have used frequency modulation.[2, 4, 5]

The aim here is to compare the two capacitive-transducer methods and to describe an instrument based on the amplitude-modulation method.

When frequency modulation is used, the probe capacitance is part of the frequency-determining resonant circuit, so that the operating frequency is

$$f = \frac{1}{2\pi\sqrt{L(C_p + C)}}, \tag{1}$$

where L is the inductance of the tank circuit, C_p is the probe capacitance, and C is the total remaining capacitance of the tank circuit, including the stray capacitance of the wiring. The sensitivity to changing probe capacitance is hence

$$\frac{df}{f} = -\frac{1}{2}\frac{dC_p}{C_p + C}. \tag{2}$$

A probe suitable for use on laboratory animals might have a tip, 1 mm in diameter, located 1/4 mm from the vibrating part. The value of C_p, with air as a dielectric, will then be 3×10^{-2} pF and its change, for vibrations of the ear of 100 Å (that is, well below the threshold of pain), will be 1×10^{-6} pF. One also assumes that the carrier

signal is in the VHF range so that the tank-circuit capacity will be relatively small (for example, 5 pF). With these assumptions, the measuring apparatus has to discriminate $\frac{df}{f} = \frac{1}{10^7}$, which requires a rather elaborate device.

For the amplitude-modulation method, the carrier-signal voltage amplitude at the input of the measuring channel is[6]

$$V_i \cong V_o \omega R_i C_p, \tag{3}$$

and the amplitude of modulation dV_i, because of the change of the probe capacitance dC_p, is

$$dV_i \cong V_o \omega R_i dC_p, \tag{4}$$

where V_o is the output amplitude of the carrier-signal generator, ω is the angular frequency, and R_i is the input impedance of the measuring channel, assumed to be resistive. The sensitivity depends on obtaining a low signal-to-noise ratio at the input of the measuring channel. This can be controlled by proper selection of the factors: V_o, ω and R_i, and by a special arrangement of the input stage. The inherent advantage of the AM mode is that the sensitivity is proportional to the ratio of the change of the probe capacitance to its static value, $dV_i/V_i = dC_p/C_p$.

The design presented here differs from the previously developed instrument,[3] mainly in two respects: (a) the sensitivity is increased so as to work with a smaller probe (diameter 1 mm) suitable for use in the middle ear of cats, and (b) a special ground arrangement was used to allow for grounding the animal. Experimental conditions with human temporal bones[3] allow the preparation to be kept floating with respect to radiofrequency potentials. In animal experiments, the animal is grounded or its capacity to ground is so large that it presents, practically, a short circuit for the radiofrequency signals.

The sensitivity of the instrument might be increased (see Eq. 4) by raising the values of V_o, ω, and/or R_i. Higher V_o and R_i produce greater carrier amplitudes in the input, and thus require a higher dynamic range of the radiofrequency amplifier. To avoid this difficulty, the carrier from the RF generator is delivered to both sides of a differential input of the RF amplifier (Fig. XXV-5). One input terminal receives the signal through the probe capacitance C_p, the other through an adjustable trimmer C_p', set near the quiescent value of the probe capacitance. This arrangement cancels (to the desired extent) the in-phase carrier signals at the input of the RF amplifier, while the amplitude modulation that is introduced by the vibrations, appears in one side only. The differential input incorporates two IF filters, which were chosen to be of high input impedance, and to operate at 455 kc. As mentioned above, both the high impedance and high frequency serve to increase sensitivity. The narrow-band frequency characteristic

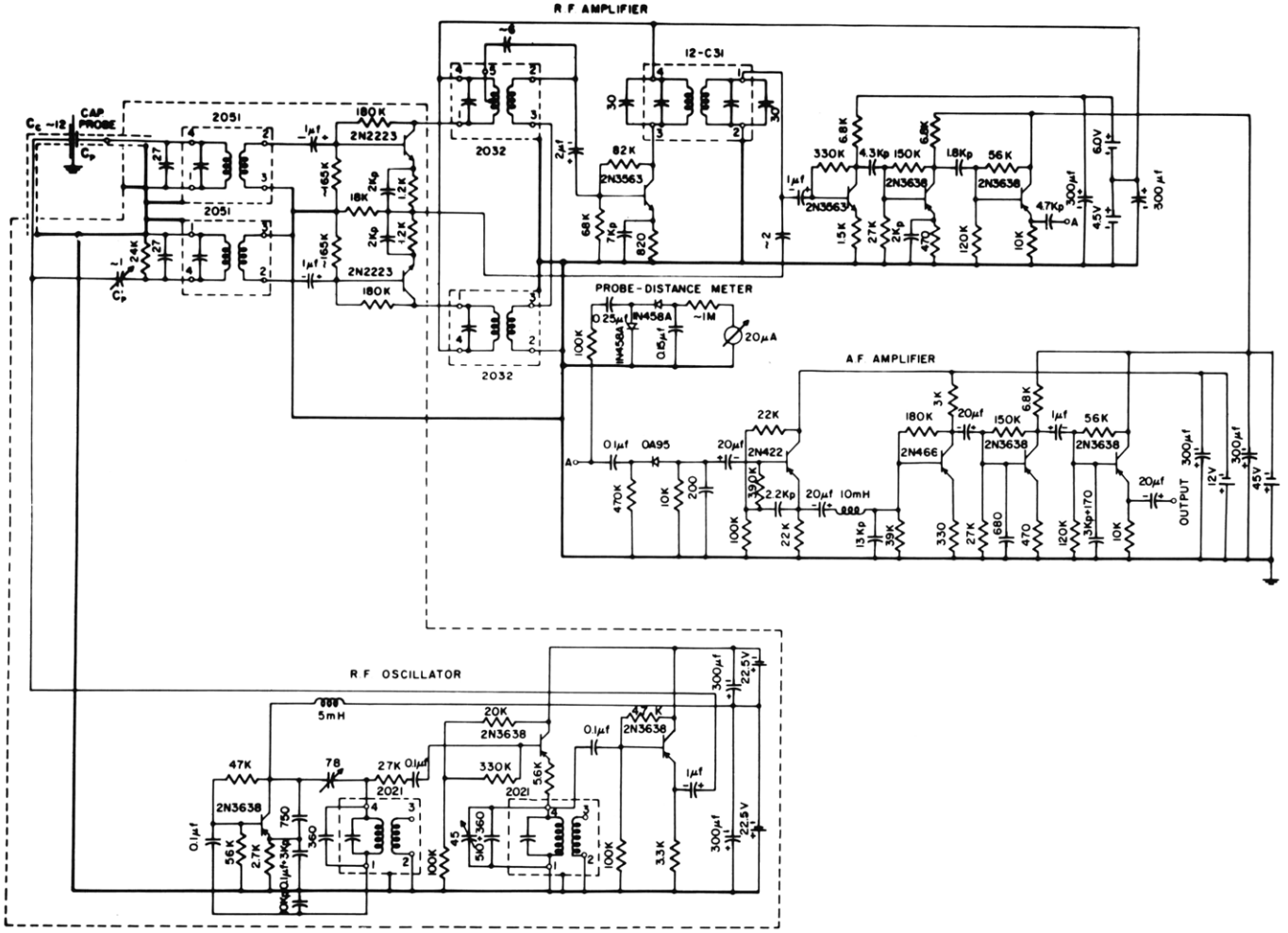

Fig. XXV-5. Circuit diagram of the capacitive-probe vibration meter. The grounded plate between the coupling capacitance C_c and the probe-capacitance C_p represents the animal.

of the filters is useful in avoiding distortion of the processed signal.

To neutralize the effect of grounding the animal, two independent common leads were provided within the instrument network, and the carrier signal from the RF generator is led to the animal through a coupling capacitance ($C_c \cong 12$ pF), which is much larger that the probe capacitance C_p (Fig. XXV-5). The input IF filters isolate the two common leads from each other. One common lead serves the RF generator and the primary windings of the input-IF filters, the other serves the secondary input-IF windings and the RF and AF amplifiers; the last common lead can be grounded. Inevitably, perfect isolation between the common leads is not possible, but means are available to cancel the influence of parasitic capacitances. This is done by tuning the coupling trimmer C'_p to bring the carrier signal in the RF amplifier to a given level, when the capacitive probe is not coupled to the vibrating surface. Bringing the probe closer to the vibrating surface causes, at first, decreasing carrier amplitude until, at a small distance (preferably a few millimeters), a minimum is reached; from that point on, the carrier amplitude rises in inverse proportion to the distance from the probe to the vibrating surface.

Some characteristics of the performance of the instrument will be noted here.

The RF oscillator is a two stage Colpitts circuit. The third stage is an emitter follower; it provides low output impedance for the constant-voltage generator. The operating frequency is 407, 830 cps; it remains stable within ±12 cps during 2 hours of work. The voltage amplitude is 16 V; it remains constant, and the signal pattern remains undistorted, for a lead at the terminals of the output coaxial cable of up to ~80 pF.

The RF amplifier presents a flat frequency characteristic (within 3 db, measured through a series 10 MΩ resistor) from 396.5 kc up to 408.5 kc. The voltage gain at 406 kc is 42, the input impedance is 205 KΩ. The frequency passband of the amplifier was fitted to allow passage of only one of the sidebands of the modulated carrier.

The output of the RF amplifier (A in Fig. XXV-5) is fed to two circuits: a network monitoring the distance of the probe from the vibrating surface, and an audiofrequency amplifier. The probe-distance meter indicates the magnitude of the carrier signal in the quiescent position of the measured part. The audio amplifier is driven by the low-frequency component of the rectified amplitude-modulated carrier. The frequency characteristic of the audio amplifier is flat (within 3 db) in the range from 10 cps up to 15 kc. The voltage gain is 70. The last (emitter-follower) stage provides low output impedance for convenience in displaying or recording the output signal.

Based on the data presented above, the inherent inaccuracy of the measuring procedure can be evaluated. The probe capacitance is between two plates, one the probe and the other the vibrating member of the ear. Thus (in accordance with Eq. 3) the voltage (V_i) can be expressed in the form

$$V_i = k \cdot \frac{1}{x}, \tag{5}$$

where k is a constant, and x is the distance between the probe and the vibrating surface. This hyperbolic dependence causes nonlinear distortion of the modulation envelope. As a figure of merit, consider the ratio of modulation amplitude in one (positive) direction $\Delta V_i'$ with respect to the other (negative) direction $\Delta V_i''$. For the changes of distance $\pm\Delta x$, this figure is

$$\frac{\Delta V_i'}{\Delta V_i''} = \frac{x + \Delta x}{x - \Delta x}. \tag{6}$$

The deviation from the condition of linearity $\Delta V_i'/\Delta V_i'' = 1$, for $|\Delta x| \ll x$, is

$$D_l = \left| 1 - \frac{\Delta V_i'}{\Delta V_i''} \right| \cong \frac{2\Delta x}{x}. \tag{7}$$

For x = 0.2 mm and Δx 1 micron, the deviation from linearity is 1 per cent.

With reference to possible effects of the carrier potentials appearing between the "plates" of the probe capacitance, the following matters should be noted. The carrier voltages are much too low to cause dielectric breakdown problems. Also the carrier frequency is far beyond the response range of the mechanical system of the ear, so there should not be any appreciable interference with the response to audio frequencies resulting from the electrostatic forces between the "plates."

A preliminary experiment was carried out on a cat. The ear of the cat was stimulated by a 1000-Hz signal; vibrations of the malleus were measured at moderate sound level.

H. Fischler

References

1. G. von Békésy, "Über die Messung der Schwingungsamplitude der Gehörknöchelchen mittels einer kapazitiven Sonde," Akust. Z. 6, 1-16 (1941).
2. I. Kirikae, The Structure and Function of the Middle Ear (University of Tokyo Press, Tokyo, Japan, 1960).
3. H. Fischler, E. H. Frei, M. Rubinstein and D. Spira, "Measurement of Sound Transmission in the Middle Ear," Fifth International Conference on Medical Electronics, University of Liége, Liége, Belgium, 1963, pp. 436-447.
4. A. R. Møller, "Transfer Function of the Middle Ear," J. Acoust. Soc. Am. 35, 1526-1534 (1963).
5. L. O. Hoeft, G. Ackerman and A. Anthony, "Measurement of the Displacements and Nonlinearities of the Guinea-Pig Tympanum," J. Acoust. Soc. Am. 36, 1836-1844 (1964).
6. H. Fischler et al., op. cit., see Eq. 3.

E. ELECTRICAL IMPEDANCE MEASUREMENTS ON CHICK CEREBRAL CORTEX IN CULTURE

1. Introduction

Electrical impedance measurements on animal tissue have been carried out for a variety of reasons[1] and vary from gross limb-to-limb measurements to relatively microscopic measurements on nerve-cell membranes. The use of impedance measurements, both in a clinical environment and in research to obtain information about tissue function and structure, has been plagued chiefly by two problems. One is electrode phenomena, and the other is the conglomerate result of the measurement. An example of the latter is the measurement of blood impedance with the electrodes placed on the arm. The measurement combines the impedance of several layers of tissue with that of the blood, possibly obscuring the desired information.

On the other hand, impedance measurement has an advantage of simplicity (provided the problems of electrode surface phenomena are avoided), often requiring no puncture, sampling or other alteration of the tissue. This advantage is important in research because the measurement need not terminate an experiment, as a histological examination or a chemical analysis might. The disadvantage of the conglomerate effect can sometimes be avoided by employing a wide frequency range in the measurement. It is then often possible to separate out the required information. The electrode surface problems can also be avoided or minimized by various methods.[2] A four-electrode technique for accomplishing this is discussed in the appendix.

The purpose of the present work is to relate impedance data, taken over the frequency range 5 Hz-200 kHz, to a structural model of tissue explants from embryonic chicken cortex. This provides a tool yielding information about the tissue structure during the course of an experiment, and, additionally, we hope that the results of the impedance measurements will have more general implications regarding the structure of nervous tissue. The structure that we refer to here includes nothing below the level of the gross structure of a cell. It is characterized by cell membrane capacities and resistances, the resistances of the extracellular and intracellular fluids, the volume densities of the various populations of cells and the cell shapes. There are many combinations of these parameters that might fit the impedance data, so that it is convenient to restrict the range of values to initiate the analysis. Fortunately, these quantities have been extensively discussed, and, under the assumption that the chicken embryo nervous tissue does not quantitatively differ too widely from that of the other more generally studied animals, a preliminary analysis of the data shows them to be consistent with the range of the reported values. A more complete analysis is awaiting histological studies of the tissue.

2. Tissue Explant and Chamber

The tissue studied is excised from the telencephalic area of the cerebral cortex of 14-day chicken embryos. An explant is 1-4 mm^3 in volume, and is sliced from the cortex surface with its base broader than its height. At this age, differentiation is complete and we are dealing with cells that are probably much as they are in the adult chicken. The general method of culturing these samples and the spontaneous electrical potentials that are recorded have been reported on previously.[3] The chamber used for the impedance measurements differs from the chambers usually employed, in that it has two (rather than one) sintered-glass blocks electrically insulated from each other with the tissue bridging the two (see Fig. XXV-6).

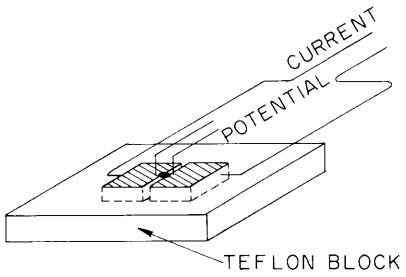

Fig. XXV-6. Split-block chamber. Tissue lies in the center and bridges the two sintered-glass blocks.

Recordings of the spontaneous potentials from the tissue are made by connecting to the current electrodes. A typical DC recording is shown in Fig. XXV-7.

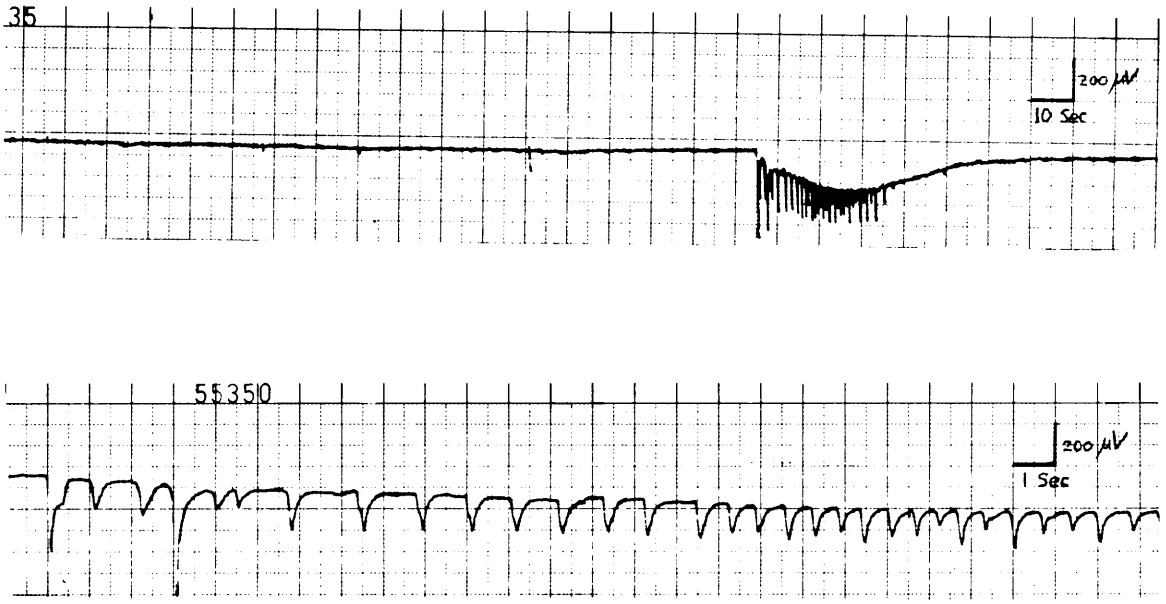

Fig. XXV-7. Typical spontaneous potential recorded from the current electrodes of the chamber in Fig. XXV-6. The lower tracing presents a portion of a sequence like the one in the upper trace in an expanded time scale.

The recordings compare in form with those made on previous occasions with microelectrodes and also with gross electrode recordings (AC) if the slow shift in the base line is deleted. The amplitudes recorded in this way are 5-10 times that of those reported from gross electrodes. The reason for this is that the split-block arrangement shown in Fig. XXV-6 avoids the considerable amount of current shunting through the sintered-glass block and fluid reservoir occurring in the single-block chambers.

3. Model and Analysis

The model assumed for the tissue explant follows the work of Ranck,[4] and details are given in his paper. An equivalent circuit for the tissue based on this model is shown in Fig. XXV-8a. R'_o represents the path through the extracellular fluid and each

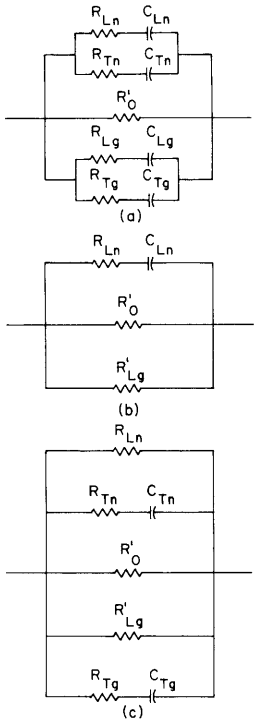

Fig. XXV-8. (a) Equivalent circuit of the tissue.
(b) Circuit at low frequencies.
(c) Circuit at high frequencies.

series R-C branch, a path involving cellular membranes. The model takes into account fibers of neuronal and glial cells that are either transverse or longitudinal to the current-flow direction. The subscripts L and T refer to longitudinal and transverse, respectively, and the second subscripts n and g, to neuronal and glial. An R-C branch represents the combination of the membrane and intracellular fluid, so that R and C are both frequency-dependent. Only R'_o is frequency-independent, in general. Because of the low membrane resistance of the glial fibers, however, the longitudinal glia can be reduced to a frequency-independent resistance, R'_{Lg}, over

the range of frequencies investigated.

The circuit of Fig. XXV-8a can be considered in a low-frequency version, Fig. XXV-8b, and a high-frequency version, Fig. XXV-8c, which greatly simplifies the analysis. As indicated in this figure, the variation at low frequencies is governed by the longitudinal neurons in parallel with the frequency-independent R'_o and R'_{Lg}, and the high-frequency variation by the transverse fibers of both cell populations in parallel with R_{Ln}, R'_o and R'_{Lg}.

Figure XXV-9 shows the real and imaginary parts of the tissue impedance for two

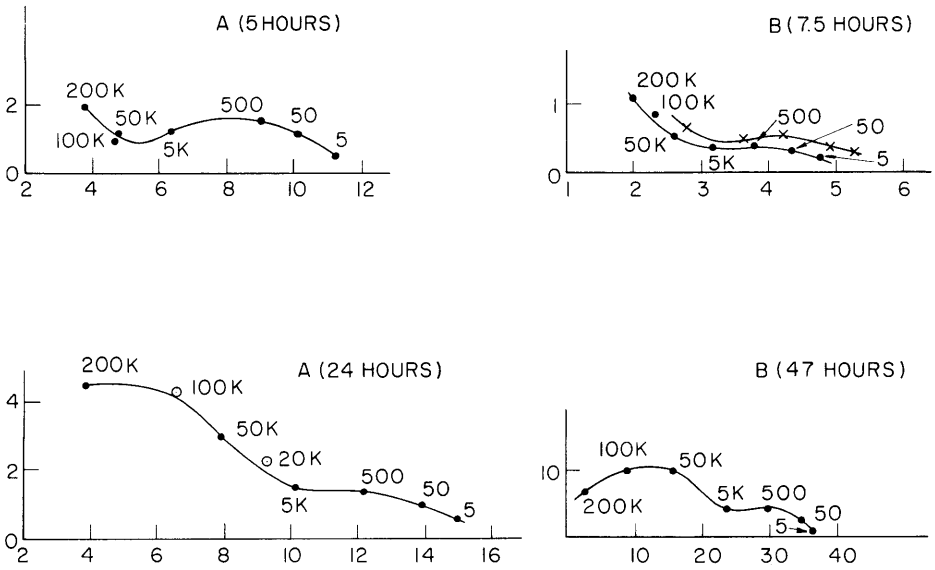

Fig. XXV-9. Real (abscissa) and imaginary (ordinate) parts of tissue impedance in KΩ. The frequencies are marked in Hz.

samples at two different times after excision, as noted. The analysis for the longitudinal fibers is made by solving the cable equation, subject to a constant-gradient sinusoidal potential in the external fluid (see Ranck[4] for details). The result of this analysis is a loop in the impedance plane similar to the low-frequency loops shown in Fig. XXV-9. The data loop can be matched with the calculated loop at the zero- and infinite-frequency points and at the point of maximum reactance.

The high-frequency loop, attributed to the presence of transverse fibers, can be analyzed by considering an expression of the Maxwell variety for a suspension of transverse cylinders in a conducting medium. Again, the calculated and experimental loops are matched, although, in this case, the experimental loop is not complete at the highest frequency (200 kHz) that was used.

A preliminary analysis of impedance data reveals the following values for several

of the parameters involved. Under the assumption that the tissue sample bridging the two sintered-glass blocks roughly forms a segment of an annulus, the specific impedance for several samples varies in the range 200-700 ohm-cm for a fresh sample (up to 7 hours after excision) at 500 Hz. With some of Ranck's calculations for the rabbit cortex employed in this preliminary analysis, the membrane time constant comes to 8 msec, which yields a membrane capacitance of 2.7 $\mu f/cm^2$ for a membrane resistance of 3×10^3 ohm-cm^2. The volume density of neurons is calculated to be 0.6. The high-frequency loop yields further information, although nothing further will be reported here, except to say that the gross aspects of the loop are consistent with the analysis.

Figure XXV-10 shows the impedance of an explant inexpertly excised and handled so

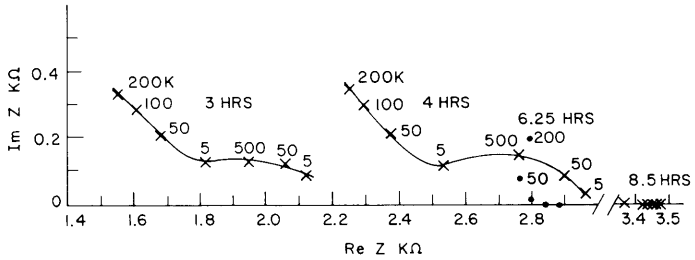

Fig. XXV-10. Tissue impedance.

that the culture did not "take." The impedance was measured at the times indicated after excision and, although it initially exhibits the usual double dispersion, it proceeds towards the real axis after a few hours, finally becoming completely resistive. This is believed to demonstrate cellular breakdown over this period of time; that is, as the cellular structures either break down or become permeable to the ions involved, the tissue exhibits the resistive character of an electrolyte. Spontaneous signals like those of Fig. XXV-7 were not observed from this tissue. On several occasions the disappearance of the spontaneous activity was observed to be accompanied by the disappearance of the loop structure in the impedance.

The model and analysis referred to above serve as a preliminary step in this investigation. The next steps already in progress are morphological studies of the tissue samples and more critical evaluation, and consequent improvement, of certain aspects of the model.

Appendix. Four-Terminal Bridge Impedance Measurement[5]

The circuit for the bridge employed in the course of these measurements is shown in Fig. XXV-11. Care was exercised in keeping the termination balanced with respect to ground, and a final amplitude balance is afforded by a movable tap on the 1.5-ohm resistor (a 3-cm piece of nichrome wire). The portion of the circuit within the dashed

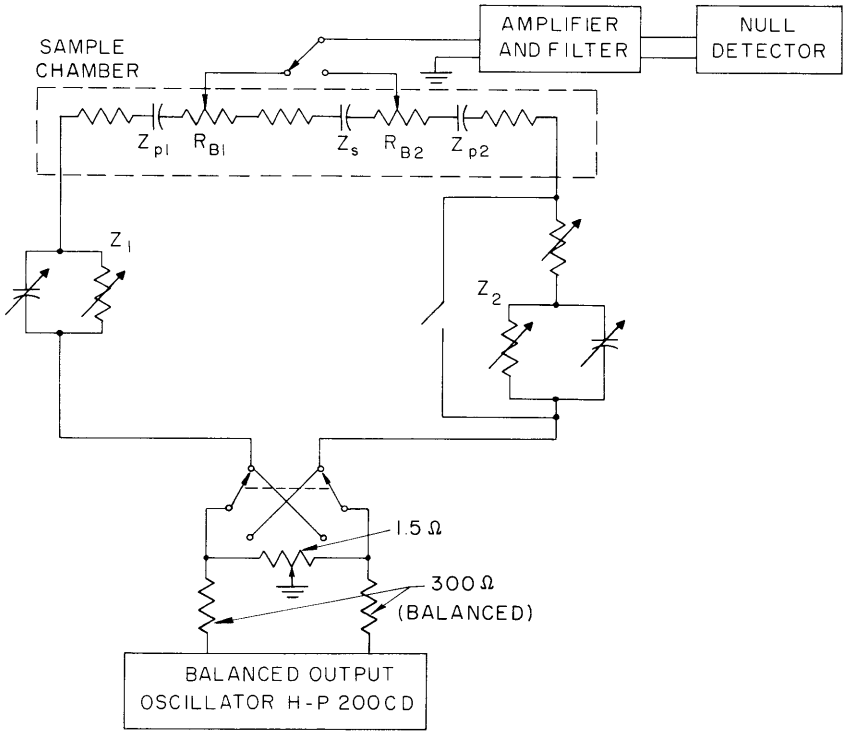

Fig. XXV-11. Four-terminal bridge.

lines is the combined equivalent circuit of the tissue sample (Z_s), the fluid-filled sintered-glass blocks (R_{b1} and R_{b2}), and the metal-electrode-fluid junctions of the current electrodes (Z_{p1} and Z_{p2}). The potential electrodes rest on the sintered-glass blocks adjacent to the tissue. (Refer also to Fig. XXV-6.)

Two balances are required to obtain the tissue impedance. In the initial balance, $Z_2 = 0$ (the shorting switch is closed) and Z_1 is adjusted for a null at the left-hand potential electrode. Thus,

$$Z_1 + Z_{p1} + R_{b1} = Z_s + R_{b2} + Z_{p2}.$$

There is a small error caused by the portion of R_{b1} lying between the potential electrode and the tissue, but this is neglected. By allowing Z_1 to remain unchanged, the second balance is made by adjusting Z_2 for a null at the other potential electrode. Then

$$Z_1 + Z_{p1} + R_{b1} + Z_s = R_{b2} + Z_{p2} + Z_2,$$

and combining the two balance conditions yields

$$Z_s = \frac{1}{2} Z_2.$$

Hence, the effects of the current-electrode impedances are avoided by employing two balances. Additionally, errors attributable to the potential-electrode impedances are avoided because each is nulled when in use.

The effects of other errors in the measurements, especially at the high-frequency end, have been assessed. One major cause of error is unbalance of the generator output. If this unbalance is small, however, the resulting error can be largely corrected by performing a second measurement with the generator output reversed and averaging the two. Stray capacitance is another source of error, and this has been minimized by the use of the very low value of driving resistance (1.5 ohm).

G. F. Songster, R. R. Rojas-Corona, A. W. B. Cunningham

References

1. L. A. Geddes, "The Transduction of Physiological Events," Chapter 2 in Advances in Bioengineering and Instrumentation, Fred Alt (ed.) (Plenum Press, New York, 1966).
2. H. P. Schwan, "Determination of Biological Impedances," Chapter 6 in Physical Techniques in Biological Research 6, W. L. Nastuk (ed.) (Academic Press, New York, 1963).
3. A. W. B. Cunningham, "Qualitative Behavior of Spontaneous Potentials from Explants of 15-day Chick Embryo Telencephalon in vitro," J. Gen. Physiol. 45, 1074 (1962).
4. J. B. Ranck, "Specific Impedance of Rabbit Cerebral Cortex," and "Analysis of Specific Impedance of Rabbit Cerebral Cortex," J. Extpl. Neurol. 7, 144-174 (1963).
5. P. H. Hill, Personal communication in which the four-terminal bridge configuration was suggested.

F. CENTRAL ORIGIN OF ASYMMETRY IN THE CAROTID SINUS REFLEX

It is known that the carotid sinus reflex mechanism brings forth asymmetrical responses for rising and falling blood pressures. One manifestation of these asymmetrical responses is that a rise in blood pressure is more effective in slowing the heart than a similar drop in blood pressure in accelerating it.[1] Although the nonlinear characteristics of the pressure receptors and the heart contribute to this asymmetry, it has been suggested that these characteristics alone are not sufficient to account for all the asymmetry in the heart response. This report presents direct evidence that the input-output characteristics of the vasomotor center also contribute to the asymmetry in the heart-rate response.

The activity of cardiac vagal efferent fibers was recorded during short transient disturbances in the arterial blood pressure of chloralose-anaesthetized dogs. These disturbances were introduced either by the injection of Levophed, or by inflating and then deflating a balloon that had been placed into the abdominal aorta of the experimental

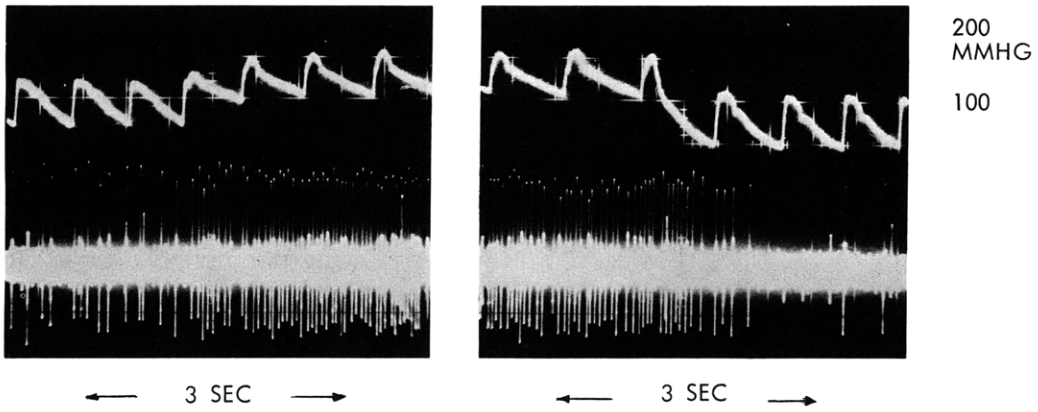

Fig. XXV-12. Single-fiber cardiac vagal efferent recording. Upper: blood pressure. Lower: nerve firing. Left: records obtained during a rise in pressure level, caused by the inflation of a balloon in the abdominal aorta. Right: records obtained during a fall in pressure level, caused by the deflation of the balloon. Elapsed time between inflation and deflation, 5 sec.

animal. The cardiac efferent fibers were dissected from the trunk of the cervical vagus, and they were identified on the basis of their firing pattern, as described by Jewett.[2]

Figure XXV-12 shows the firing of a typical cardiac vagal efferent fiber during sudden changes of blood pressure. While the response to the rise in pressure level following the inflation of the balloon is evident in approximately 100 msec, there is a delay of approximately 300 msec before the response to the rapidly falling pressure after the deflation of the balloon commences. Firing continues for almost a full beat after the precipitous drop in the pressure. In contrast, the afferent activity of the pressure receptors show an essentially instantaneous response both to rising and falling blood pressures as a result of the rate-sensitivity of these receptors.[3] The findings, therefore, indicate that the time delay before a change in baroreceptor firing affects vagal efferent firing is larger for decreasing than for increasing pressures.

Occasionally, vagal fibers have such a high threshold under the studied experimental conditions, that they fire only when the pressure is elevated, as shown in Fig. XXV-13. These fibers can exhibit a very pronounced asymmetry in their response to rising and falling pressures. Figure XXV-14 shows the changes in vagal activity of a multi-fiber vagal preparation during a transient pressure disturbance. The firing frequency increased while the pressure level was climbing, but then it gradually decreased to its original value. No change in firing frequency occurred when the pressure suddenly decreased as a result of deflating the balloon, although the decrease in pressure did initiate a heart-rate response. This response was probably mediated predominantly by the sympathetic nerves. Since the vagus nerves are more effective

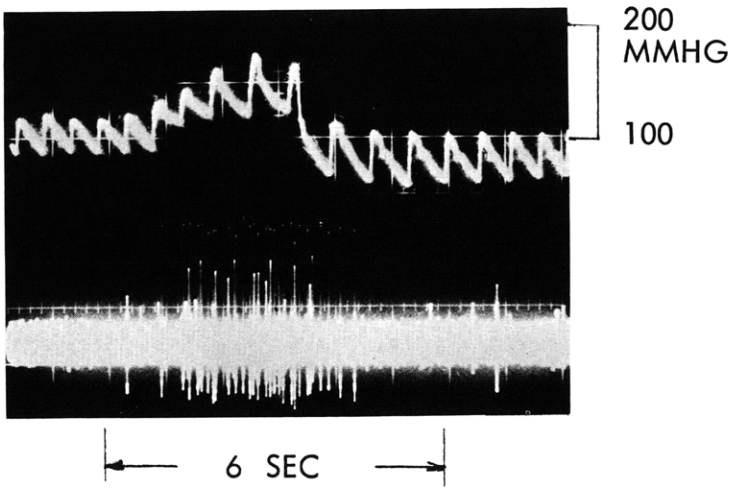

Fig. XXV-13.

Threshold for vagal activity. Upper: blood pressure during a short inflation of the balloon. Lower: nerve firing. Vagal activity (considering the fiber giving the largest spike amplitude) is present only as a result of the elevated pressure.

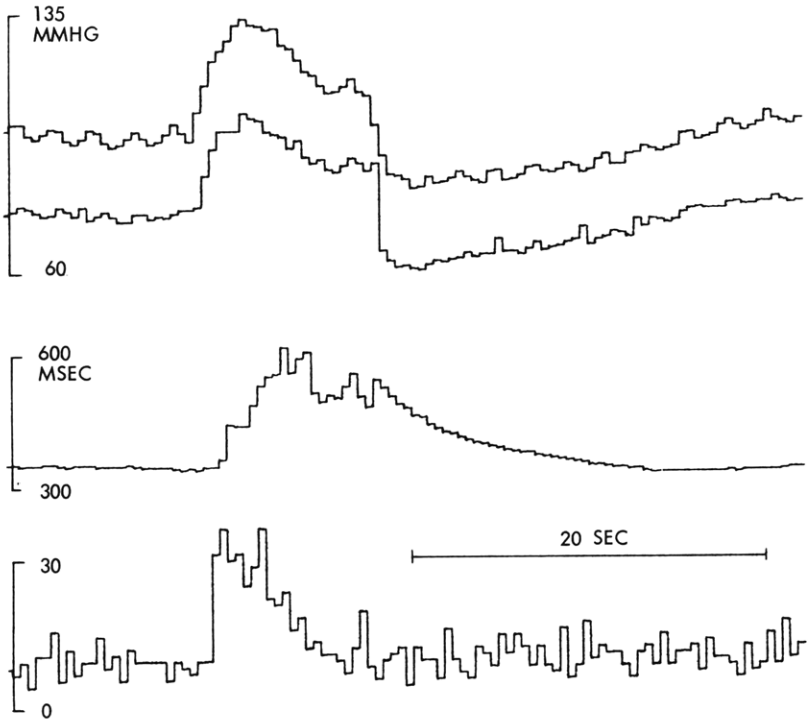

Fig. XXV-14. Vagal activity and heart period during a rise and fall of blood pressure. From top to bottom: systolic pressure, diastolic pressure, heart period, and vagal activity. The record was obtained with the aid of a digital computer; all four quantities were computed and displayed on a beat-by-beat basis. Heart period was computed as the time interval between neighboring QRS complexes in the electrocardiogram. Vagal activity was measured as the number of firings in each heart beat within a 320-msec interval following the QRS complex.

than the sympathetic ones in causing rapid changes in the speed of the heart,[1,4] the asymmetry in the vagal firing frequency for rising and falling pressures resulted in a marked asymmetry in the heart-rate response.

The decrease of vagal firing during the elevated pressure level may have been caused by the adaptation of the baroreceptors, coupled with a threshold for introducing changes in the vagal firing frequency. This could account for the observed behavior shown in Fig. XXV-14. It only need be assumed that in the multi-fiber preparation one or more high-threshold cardiac efferent fibers were among other types of fibers that did not change their firing frequency as a result of blood-pressure changes. (Fibers of this type in the trunk of the cervical vagus have been described.[2]) Adaption of the vagus center, the possibility of which has been suggested by Wang and Borison,[4] may also have been a factor in producing the decreasing firing frequency indicated in Fig. XXV-14.

The technical help of Messrs. Nicholas Pantelakis, Brian S. Terry, and James W. Poitras was invaluable in obtaining the nerve recordings.

P. G. Katona

References

1. P. G. Katona, "Computer Simulation of the Blood Pressure Control of Heart Period," Sc.D. Thesis, Department of Electrical Engineering, M.I.T., June 1965.

2. D. L. Jewett, "Activity of Single Efferent Fibres in the Cervical Vagus Nerve of the Dog with Special Reference to Possible Cardio-inhibitory Fibres," J. Physiol. 175, 321 (1964).

3. S. Landgren, "On the Excitation Mechanism of the Carotid Baroreceptors," Acta Physiol. Scand. 26, 1 (1952).

4. S. C. Wang and H. L. Borison, "An Analysis of the Carotid Sinus Cardiovascular Reflex Mechanism," Am. J. Physiol. 150, 712 (1947).